Nanoscale

COMMUNICATION

View Article Online
View Journal | View Issue



Cite this: *Nanoscale*, 2018, **10**, 118

Received 21st August 2017,
Accepted 21st November 2017

DOI: 10.1039/c7nr06219b

rsc.li/nanoscale



# Design of a wearable and shape-memory fibriform sensor for the detection of multimodal deformation†

Li Li,[a] Peipei Shi,[a] Li Hua,[a] Jianing An,[b] Yujiao Gong,[a] Ruyi Chen,[a] Chenyang Yu,[a] Weiwei Hua,[a] Fei Xiu,[a] Jinyuan Zhou,[c] Guangfa Gao,[d] Zhong Jin,[e] Gengzhi Sun*[a] and Wei Huang*[a,f]

**A wearable and shape-memory strain sensor with a coaxial configuration is designed, comprising a thermoplastic polyurethane fiber as the core support, well-aligned and interconnected carbon nanotubes (CNTs) as conductive filaments, and polypyrrole (PPy) coating as the cladding layer. In this design, the stress relaxation between CNTs is well confined by the outer PPy cladding layer, which endows the fibriform sensor with good reliability and repeatability. The microcracks generated when the coaxial fiber is under strain guarantee the superior sensitivity of this fibriform sensor with a gauge factor of 12 at 0.1% strain, a wide detectable range (from 0.1% to 50% tensile strain), and the ability to detect multimodal deformation (tension, bending, and torsion) and human motions (finger bending, breathing, and phonation). In addition, due to its shape-memory characteristic, the sensing performance of the fibriform sensor is well retained after its shape recovers from 50% deformation and the fabric woven from the shape-memory coaxial fibers can be worn on the elbow joints in a reversible manner (original-enlarged-recovered) and fitted tightly. Thus, this sensor shows promising applications in wearable electronics.**

## Introduction

As an important subfield of smart textiles, wearable strain sensors with high sensitivity, wide detection range, and ability to detect multimodal deformations have attracted significant interest due to their potential applications in electronic skins, motion capture, personal protection, and health care.[1–4] Although conventional strain gauges based on metallic materials exhibit high sensitivity due to the micro/nano-cracks generated under tiny strain, they severely suffer from poor mechanical compliance and a narrow sensing range (normally less than 5% strain), making them incompetent for use in wearable electronics.[5]

To overcome the aforementioned drawbacks, alternative nanostructures such as metal nanowires,[6,7] graphene,[8–11] and carbon nanotubes (CNTs)[12–14] have been adopted as newly developed sensing materials. Among these candidates, CNTs are preferred for the fabrication of high-performance strain sensors due to their one-dimensional structure, superior mechanical strength, low electrical resistivity, and ability to form conductive networks.[15] Moreover, one of the widely utilized approaches is to incorporate CNTs into a rubbery matrix through a solution blending method.[16] When the sensor is subjected to mechanical deformation, the interconnection between CNTs in the matrix changes; this provides a responsive signal with respect to electrical conductance. However, one unresolvable issue lies in obtaining a good dispersion of CNTs, which determines the sensing performance of the resulting devices.[17] Besides, the incorporation of CNTs into the polymer matrix inevitably increases the stiffness of the composite and thereby narrows the sensing range of the device.[18–20] Another strategy is to deposit pre-formed CNT networks, *e.g.*, interconnected CNT sheets, on top of an elastomer substrate.[21] The interconnection between CNTs in such sheets primarily arises from weak van der Waals forces.[22–25] However, under conditions of large strain or repetitive loading-unloading cycles, the as-fabricated sensors exhibit poor stability and repeatability, as well as inferior sensitivity to small defor-

[a]*Key Laboratory of Flexible Electronics (KLOFE) & Institute of Advanced Materials (IAM), Jiangsu National Synergetic Innovation Center for Advanced Materials (SICAM), Nanjing Tech University (NanjingTech), 30 South Puzhu Road, Nanjing 211816, P. R. China. E-mail: iamgzsun@njtech.edu.cn, iamwhuang@njtech.edu.cn*
[b]*School of Mechanical and Aerospace Engineering, Nanyang Technological University, 50 Nanyang Avenue, 639798, Singapore*
[c]*School of Physical Science and Technology, Lanzhou University, 222 South Tianshui Road, Lanzhou 730000, P. R. China*
[d]*School of Mechanical Engineering, Nanjing University of Science and Technology, 200 Xiao Ling Wei, Nanjing 210094, P. R. China*
[e]*Key Laboratory of Mesoscopic Chemistry of MOE, School of Chemistry and Chemical Engineering, Nanjing University, 163 Xianlin Avenue, Nanjing 210023, P. R. China*
[f]*Shannxi Institute of Flexible Electronics (SIFE), Northwestern Polytechnical University, 127 West Youyi Road, Xi'an 710072, P. R. China.*
*E-mail: iamwhuang@njtech.edu.cn*

†Electronic supplementary information (ESI) available. See DOI: 10.1039/c7nr06219b

mation, due to the sliding between CNTs as a result of stress relaxation.[21] In addition, the majority of precedent strain sensors are incapable of sensing multimodal deformations (*e.g.*, stretching, bending and twisting) simultaneously, which hinders their application in the detection of complex body movements.[26] Furthermore, most of the reported strain sensors are built on planar substrates, which make them unable to be tightly fitted onto complex/irregular three dimensional (3D) architectures, such as elbow joints and knee joints. This poses problems in electronic sensing of the dynamic motions of the human body.[26]

Herein, for the first time, we develop a shape-memory fiber sensor with a coaxial configuration consisting of thermoplastic polyurethane (TPU) fiber as the core-support, well-aligned CNTs as conductive filaments, and polypyrrole (PPy) coating as the cladding layer. In this design, the stress relaxation between CNTs is well confined by the outer PPy layer, which endows the fibriform sensor with good reliability and repeatability. On the other hand, the microcracks generated when the coaxial fiber is under strain guarantee the fibriform sensor high sensitivity, superior detection limit and wide detectable range for multimodal deformations (tension, bending, and torsion) and human motions (finger bending, breathing and phonation). Owing to its shape-memory characteristic, the fibriform sensor maintains good sensing properties after its shape recovers from 50% deformation to the original state. As a proof-of-concept application, a fabric is further woven from the shape-memory coaxial fibers, which is worn and fitted tightly on the elbow joints in a reversible manner (original-enlarged-recovered).

## Results and discussion

The fabrication of the shape-memory fibriform sensor is schematically illustrated in Fig. 1. The spinnable vertically-aligned CNT array with a thickness of ~300 μm (Fig. S1†) was prepared through chemical vapor deposition (CVD) according to our previous studies.[27–33] The TEM image (Fig. S2†) shows that the CNTs have a mean diameter of 10 nm with multi-walls. In the Raman spectrum of the CNTs (Fig. S3†), there are two characteristic peaks at 1350 $cm^{-1}$ and 1580 $cm^{-1}$, which correspond to the D and G band, respectively. The G/D radio is about 1.05, which indicates high-quality CNTs.[28] Due to the unique interconnection between the CNTs in the array,[22–25] a well-aligned CNT sheet (Fig. S1b†) was continuously pulled out and cross-stacked on TPU fiber at an angle of 80° between the pulling direction of the CNT sheet and the axis of the TPU fiber (Fig. S4†) to obtain the TPU@CNT fiber (Step 1). Subsequently, a thin layer of PPy was electrochemically deposited on the outer surface of the TPU@CNT fiber to form the TPU@CNT@PPy (TCP) fiber (Step 2).

The conductance of the TPU@CNT fiber and TCP fiber can be facilely tuned by the number of CNT layers and electrochemical deposition time. The well-aligned characteristic of the CNT sheet gives it high conductivity.[32] As the number of cross-stacked CNT layers increases, the specific length resistance decreases from 9.4 kΩ $cm^{-1}$ for the TPU@CNT fiber with one CNT layer to 3.0 kΩ $cm^{-1}$ for the TPU@CNT fiber with four CNT layers (Fig. 2a). The outermost PPy coating was achieved by electrochemical deposition at a constant potential of 0.8 V. It is found that the resistance of the TCP fiber decreases with the deposition of PPy in a time dependent manner (Fig. 2b). The morphology change in the resultant

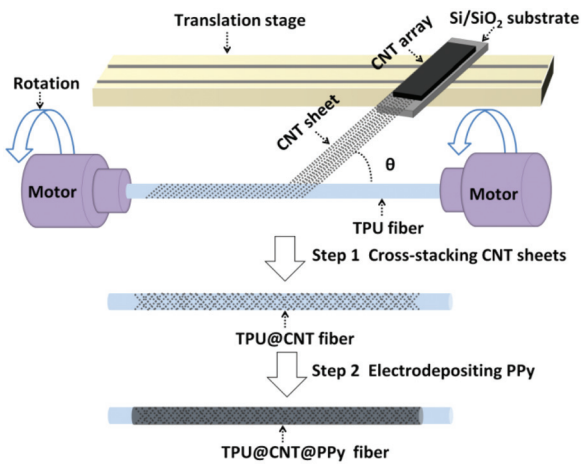


Fig. 1 Schematic showing the fabrication of the TCP fibriform sensor.

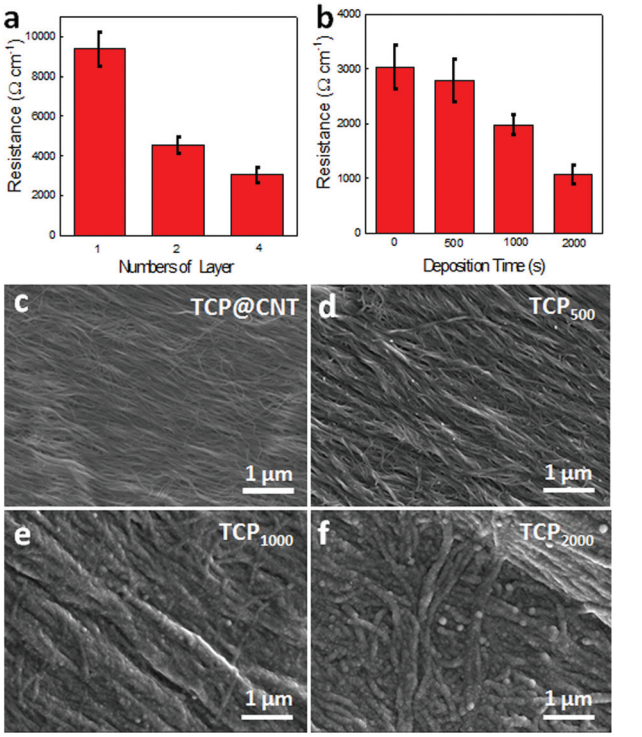


Fig. 2 (a) Resistance of the TPU@CNT fiber as a function of the number of CNT layers. (b) Resistance of TCP fibers *versus* electrochemical deposition time. (c–f) SEM images showing the morphology change of the TCP fibers (with 4 layers of CNT sheets) with respect to deposition time.

hybrid fibers with respect to deposition time was characterized using scanning electron microscopy (SEM). It can be clearly observed that on the surface of the TPU@CNT fiber, the CNTs are well-aligned in the same orientation (Fig. 2c). In comparison, the surface morphology of the TCP fiber changes gradually and the surface coating becomes thicker when the deposition time increases from 0 to 2000 s (Fig. 2d–f). Ultimately, a coralline-like structure was formed on the surface of the TCP fiber with 2000 s deposition of PPy (denoted as $TCP_{2000}$ fiber, as shown in Fig. 2f). In the cross-sectional SEM image (Fig. S5†), the coaxial structure can be observed clearly.

The strain sensing performance of the TCP fiber was tested by measuring its relative resistance variation ($\Delta R/R_0$, where $\Delta R = R - R_0$, and $R_0$ and $R$ are the resistance of TCP fiber before and after deformation, respectively) upon stretching. Compared to the TPU@CNT fiber, the TCP fibers exhibited higher sensitivity to tensile strain with a slightly compromised detectable range (Fig. 3a). Specifically, the maximum sensitivity was obtained with the $TCP_{2000}$ fiber within the strain of 60%, over which $\Delta R/R_0$ increases dramatically. This phenomenon can be attributed to the peeling-off of the PPy layer (Fig. S6†) which leads to a rapid increase in fiber resistance and ultimate failure of the fiber sensor. Therefore, unless otherwise specified, the $TCP_{2000}$ fiber was used for the following studies within the strain range of 0–50%. The sensing capability of the $TCP_{2000}$ fiber to stepwise tensile strain was examined in Fig. 3b. The $\Delta R/R_0$ value of the $TCP_{2000}$ fiber upon stretching from 10% to 50% was measured to be 55% to 150%, respectively, which is much higher than that of the TPU@CNT fiber. As a demonstration of direct visual observation, both the TPU@CNT and $TCP_{2000}$ fibers were used as conductive wire to light an LED. Compared to the that connected to the TPU@CNT fiber, the LED connected to the $TCP_{2000}$ fiber exhibited a more obvious change in brightness when the fiber was subjected to 50% strain (Fig. S7†), which indicating its superior sensitivity to large tensile strain. Besides, the $TCP_{2000}$ fiber sensor also shows the capability for the detection of tiny strain. The detection limit of the fiber sensor was determined by applying a gradually diminishing step strain (Fig. 3c). The $\Delta R/R_0$ value in response to the tiny strain of 0.1% was measured to be 1.2%, giving a gauge factor (GF) of 12, where GF is defined as $(\Delta R/R_0)/\varepsilon$ ($\varepsilon$ is the strain). This high detection limit makes the $TCP_{2000}$ fiber sensor superior to the planar sensors devised using aligned single-walled CNT films on poly(dimethylsiloxane) (PDMS),[14] hybridized films of CNT and graphene on PDMS,[34] and highly-oriented CNT fiber on PDMS.[13] It is also comparable to that of the sensor based on graphene woven fabrics on PDMS.[35] In addition, these stepwise tensile testing results within the strain range of 0.1% to 50% (Fig. S8†) are in good agreement with that shown in Fig. 3a, which suggest the good repeatability of the $TCP_{2000}$ fiber. Moreover, under cyclic tensile tests within 50% strain, the $TCP_{2000}$ fiber sensor shows good durability and stability with $\Delta R/R_0$ retention maintained above 90% after 500 loading-unloading cycles (Fig. 3d), which is of critical importance for practical applications.

The microstructures of the TPU@CNT fiber and $TCP_{2000}$ fiber during the tensile test were characterized *via* SEM (Fig. 4a–f). In the case of the TPU@CNT fiber in its original state, the CNTs are wound on TPU with good alignment (Fig. 4a). When the TPU@CNT fiber was subjected to 50% tensile strain, the CNTs became electrically disconnected (Fig. 4b) leading to an increase in fiber resistance. Due to the

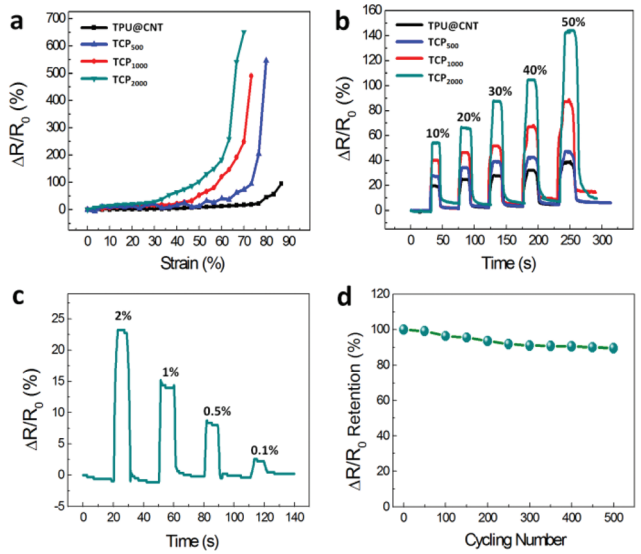


Fig. 3 (a) Electrical responses of the TPU@CNT, $TCP_{500}$, $TCP_{1000}$, and $TCP_{2000}$ fibers under tensile strain. (b) Resistance variations of the TPU@CNT, $TCP_{500}$, $TCP_{1000}$, and $TCP_{2000}$ fibers under stepwise tensile test with strain ranging from 10% to 50%. (c) Resistance variation of the $TCP_{2000}$ fiber under the small tensile strain range of 0.1% to 2%. (d) Cyclic stretching–releasing tensile test of the $TCP_{2000}$ fiber.

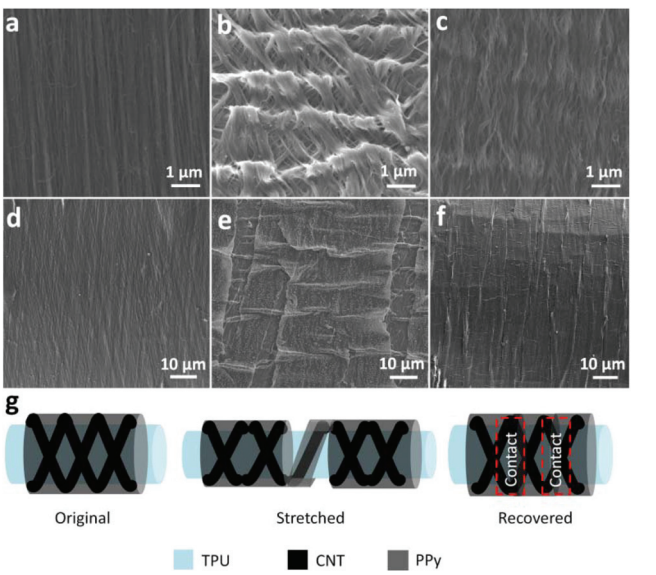


Fig. 4 SEM images of (a–c) TPU@CNT fiber and (d–f) $TPC_{2000}$ fiber in its original, 50% stretched, and released states, respectively. (g) Schematic illustration of the sensing mechanism.

irreversible sliding between CNTs under stretching,[22] the CNTs became wavy even when the TPU@CNT fiber was released to its original state (Fig. 4c), which explains its poor sensitivity and reliability. In comparison, with the presence of the PPy coating on the CNT film as a cladding layer (Fig. 4d), when the $TCP_{2000}$ fiber is under tension, microcracks are generated and the conductive filaments (CNTs) are well confined by the PPy layer (Fig. 4e). Once the applied strain is released, the microcracks are closed and the electrical connection between the CNTs is retained perfectly (Fig. 4f). Therefore, the superior sensing performance of the $TCP_{2000}$ fiber (compared to that of the TPU@CNT fiber) can be attributed to the coaxial design with the assistance of the PPy coating (Fig. 4g).

To demonstrate the potential of the $TCP_{2000}$ fiber as a wearable sensor for the detection of human activity, the fiber sensor was fixed onto the index finger and the electrical signal of $\Delta R/R_0$ was recorded in real time when the finger was gradually bent (Fig. 5a). Apparently, the increased bending magnitude leads to a steadily increased electrical response. For capturing subtle physiological signals, the wearable sensors were attached to the chest and throat. The time interval and peak amplitude in the electrical signals are presented in Fig. 5b, which were measured in the relaxation and respiration states and reflect the respiration rate and depth, respectively. Due to the complicated vocal cord vibration and muscle movements around the throat during phonation, when the tester spoke different words, such as "Hi", "Hello", and "Sensor", the response curves exhibited remarkably different characteristics with good repeatability (Fig. 5c). This indicates that the $TCP_{2000}$ fiber sensor has potential applications in speech rehabilitation training and intelligent speech recognition.[36] For sophisticated motion capture, torsion is another vital mechanical deformation in human joints and artificial muscles.[37] Benefitting from the symmetrical structure of the CNT@PPy network, the $TCP_{2000}$ fiber is capable of sensing torsion in both counterclockwise and clockwise directions at different angles with high reproducibility (Fig. 5d), which further broadens its applications in wearable electronics.

Generally, strain sensors constructed on planar substrates have only a simplex shape, which is difficult to be applied on a subject with a complex structure.[26] For instance, in practical applications, sensing devices are normally required to be fixed onto different parts of the body, *e.g.*, finger, elbow joint, and chest. Therefore, it is highly desirable to design a sensing system that can readily and tightly accommodate its shape to any complex structure in addition to the commonly used planar surface in lab testing. Fortunately, the shape-memory TCP fiber sensor developed in this study can be programmed into a variety of shapes to be adapted to different working conditions. As shown in Fig. 6a, the $TCP_{2000}$ fiber was deformed and shaped with increased radii of curvature under external bending stresses at a temperature above the glass transition temperature ($T_{trans}$).[38] After cooling to room temperature, the polymeric network of the TPU core fiber was physically cross-linked to maintain the enlarged shape.[39] Upon heating at a temperature equal to or beyond $T_{trans}$, the $TCP_{2000}$ fiber fully recovered to its original state due to the cleavage of the physical crosslinks in TPU. The sensing properties of the $TCP_{2000}$ fiber sensor and that after the shape-memory process from 50% deformation remain almost the identical (Fig. 6b), which suggests good reliability for potential practical applications. As a proof-of-concept demonstration, the textile woven from $TCP_{2000}$ fibers can be reversibly adapted into different user-required shapes and sizes, and fitted tightly to the elbow joint, as shown in Fig. 6c.

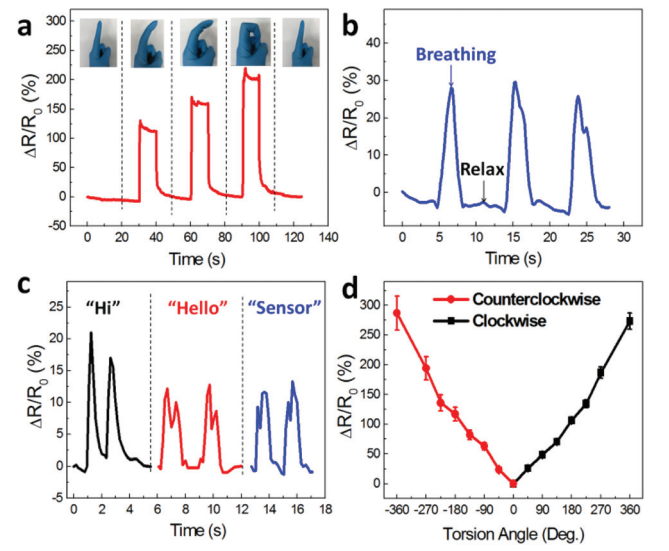


Fig. 5 Responsive signal of the $TCP_{2000}$ fibriform sensor *in situ* monitoring (a) finger bending, (b) human breathing, (c) phonation, and (d) torsion at different angles.

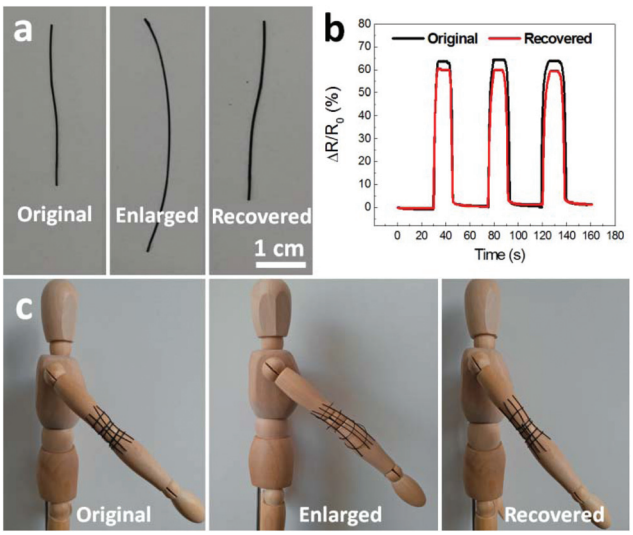


Fig. 6 (a) Images of the shape-memory $TCP_{2000}$ fibriform sensor in the original, enlarged, and recovered states. (b) Sensing behavior of the $TCP_{2000}$ fiber in the original and recovered states. (c) Photographs showing the fabric woven by the shape-memory fibriform sensors, which is tightly-fitted onto the elbow of a model.

## Conclusions

In summary, we developed a fibriform strain sensor that possesses the desirable integration of high sensitivity, broad detection range in strain, superior detection limit, and the capability of sensing multimodal mechanical deformations (tension, bending, and torsion) and monitoring human motions (finger bending, breathing and phonation). In addition, the fibriform sensor shows shape-memory characteristics enabling its fabric to be tightly-fitted to a nonplanar irregular subject, which has not been achieved by the planar strain sensors reported thus. The facile, low-cost, and dry-state fabrication process, as well as the unique coaxial architecture indicate that our fiber sensor is promising for practical applications in electronic skins, motion capture, personal protection, and healthcare.

## Experimental

### Preparation of vertically-aligned CNT arrays

Vertically-aligned CNT arrays were synthesized using a CVD process in a tube furnace.[27–33] Typically, the growth was carried out at 750 °C for 10 min using an Fe thin film (1 nm thick) deposited on an $Si/SiO_2$ substrate as the catalyst, and $C_2H_4$ and Ar as the carbon source and carrier gas, respectively.

### Fabrication of TPU@CNT fiber

Commercial TPU fiber (diameter of 500 μm) was used as the core substrate. Two ends of the TPU fiber were fixed to two electric motors, and a CNT array was stabilized on a motorized translation stage. A well-aligned CNT sheet was continuously drawn from the CNT array and wound around the fixed TPU fiber at an angle of 80° between the orientation of the CNT sheet and the axis of the TPU fiber. The two electric motors and the translation stage were operated simultaneously. The winding velocity of the aligned CNT sheet was controlled to be equal to the moving velocity of the translation stage so that the helical angle of the aligned CNT sheet was maintained across the fiber during wrapping.

### Fabrication of TCP fiber

PPy was electrodeposited onto the TPU@CNT fiber *via* the electropolymerization of pyrrole at a constant potential of 0.8 V in an aqueous solution containing pyrrole (0.05 M), KCl (0.02 M) and HCl (0.001 M), with Ag/AgCl (saturated KCl) as the reference electrode and platinum plate as the counter electrode.

### Fabrication of TCP fiber based wearable sensor

The TCP fiber (2 cm in length) was placed onto a PDMS (a 10 : 1 mixture of PDMS prepolymer and curing agent, Sylgrad-184, Dow Corning) thin film. Copper wires (0.2 mm in diameter) were connected to the two ends of the TCP fiber with the help of silver paste for *in situ* electrical tests.

### Characterization and measurement

SEM (JEOL, JSM-7800F) was used to observe the microstructure of the fiber during stretching and after testing. TEM (JEOL-2010) and Raman Spectroscopy (WITEC, Alpha300M+) with a 633 nm laser source were used to characterize the CNTs. A microforce testing system (HY-0350, Shanghai Heng Yi Precise Instrument Co., Ltd) was used to apply constant stress, strain, and displacement to the strain sensor at a loading speed of 20 mm $min^{-1}$. A digital source meter (Keithley 2400) was used to measure the relative resistance change of the sensor, and the results were recorded on a computer using LabVIEW.

## Conflicts of interest

There are no conflicts of interest to declare.

## Acknowledgements

This work was supported by NanjingTech Start-Up Grant (3983500150), Jiangsu Specially-Appointed Professor program (54935012), the Natural Science Foundation of Jiangsu Province (BK20171018) and the National Natural Science Foundation of China (61704076, 11472008 and 11674140).

## References

1 A. Chortos, J. Liu and Z. A. Bao, *Nat. Mater.*, 2016, **15**, 937–950.
2 Z. N. Bao, *MRS Bull.*, 2016, **41**, 897–902.
3 A. Chortos and Z. N. Bao, *Mater. Today*, 2014, **17**, 321–331.
4 M. L. Hammock, A. Chortos, B. C. K. Tee, J. B. H. Tok and Z. A. Bao, *Adv. Mater.*, 2013, **25**, 5997–6037.
5 J. Park, I. You, S. Shin and U. Jeong, *ChemPhysChem*, 2015, **16**, 1155–1163.
6 S. Lee, S. Shin, S. Lee, J. Seo, J. Lee, S. Son, H. J. Cho, H. Algadi, S. Al-Sayari, D. E. Kim and T. Lee, *Adv. Funct. Mater.*, 2015, **25**, 3114–3121.
7 R. Ma, B. Kang, S. Cho, M. Choi and S. Baik, *ACS Nano*, 2015, **9**, 10876–10886.
8 F. Zhao, Y. Zhao, H. H. Cheng and L. T. Qu, *Angew. Chem., Int. Ed.*, 2015, **54**, 14951–14955.
9 Y. Cheng, R. R. Wang, J. Sun and L. Gao, *Adv. Mater.*, 2015, **27**, 7365–7371.
10 Q. Liu, J. Chen, Y. R. Li and G. Q. Shi, *ACS Nano*, 2016, **10**, 7901–7906.
11 C. Y. Yan, J. X. Wang, W. B. Kang, M. Q. Cui, X. Wang, C. Y. Foo, K. J. Chee and P. S. Lee, *Adv. Mater.*, 2014, **26**, 2022–2027.
12 J. Foroughi, G. M. Spinks, S. Aziz, A. Mirabedini, A. Jeiranikhameneh, G. G. Wallace, M. E. Kozlov and R. H. Baughman, *ACS Nano*, 2016, **10**, 9129–9135.
13 S. Ryu, P. Lee, J. B. Chou, R. Z. Xu, R. Zhao, A. J. Hart and S. G. Kim, *ACS Nano*, 2015, **9**, 5929–5936.

 

14 T. Yamada, Y. Hayamizu, Y. Yamamoto, Y. Yomogida, A. Izadi-Najafabadi, D. N. Futaba and K. Hata, *Nat. Nanotechnol.*, 2011, **6**, 296–301.
15 D. J. Lipomi, M. Vosgueritchian, B. C. K. Tee, S. L. Hellstrom, J. A. Lee, C. H. Fox and Z. N. Bao, *Nat. Nanotechnol.*, 2011, **6**, 788–792.
16 S. Jung, J. H. Kim, J. Kim, S. Choi, J. Lee, I. Park, T. Hyeon and D. H. Kim, *Adv. Mater.*, 2014, **26**, 4825–4830.
17 S. Park, M. Vosguerichian and Z. A. Bao, *Nanoscale*, 2013, **5**, 1727–1752.
18 P. D. Bradford, X. Wang, H. B. Zhao, J. P. Maria, Q. X. Jia and Y. T. Zhu, *Compos. Sci. Technol.*, 2010, **70**, 1980–1985.
19 J. J. Ge, H. Q. Hou, Q. Li, M. J. Graham, A. Greiner, D. H. Reneker, F. W. Harris and S. Z. D. Cheng, *J. Am. Chem. Soc.*, 2004, **126**, 15754–15761.
20 Q. F. Cheng, M. Z. Li, L. Jiang and Z. Y. Tang, *Adv. Mater.*, 2012, **24**, 1838–1843.
21 F. Xu, X. Wang, Y. T. Zhu and Y. Zhu, *Adv. Funct. Mater.*, 2012, **22**, 1279–1283.
22 G. Z. Sun, L. X. Zheng, J. Y. Zhou, Y. N. Zhang, Z. Y. Zhan and J. H. L. Pang, *Int. J. Plast.*, 2013, **40**, 56–64.
23 X. B. Zhang, K. L. Jiang, C. Teng, P. Liu, L. Zhang, J. Kong, T. H. Zhang, Q. Q. Li and S. S. Fan, *Adv. Mater.*, 2006, **18**, 1505–1510.
24 M. Zhang, S. L. Fang, A. A. Zakhidov, S. B. Lee, A. E. Aliev, C. D. Williams, K. R. Atkinson and R. H. Baughman, *Science*, 2005, **309**, 1215–1219.
25 L. Hua, Z. Y. Ma, P. P. Shi, L. Li, K. Rui, J. Y. Zhou, X. Huang, X. Liu, J. X. Zhu, G. Z. Sun and W. Huang, *J. Mater. Chem. A*, 2017, **5**, 2483–2487.
26 M. Amjadi, K. U. Kyung, I. Park and M. Sitti, *Adv. Funct. Mater.*, 2016, **26**, 1678–1698.
27 P. P. Shi, L. Li, L. Hua, Q. Q. Qian, P. F. Wang, J. Y. Zhou, G. Z. Sun and W. Huang, *ACS Nano*, 2017, **11**, 444–452.
28 G. Z. Sun, Y. X. Huang, L. X. Zheng, Z. Y. Zhan, Y. N. Zhang, J. H. L. Pang, T. Wu and P. Chen, *Nanoscale*, 2011, **3**, 4854–4858.
29 G. Z. Sun, J. Q. Liu, L. X. Zheng, W. Huang and H. Zhang, *Angew. Chem., Int. Ed.*, 2013, **52**, 13351–13355.
30 G. Z. Sun, X. Zhang, R. Z. Lin, B. Chen, L. X. Zheng, X. Huang, L. Huang, W. Huang, H. Zhang and P. Chen, *Adv. Electron. Mater.*, 2016, **2**, 1600102.
31 G. Z. Sun, X. Zhang, R. Z. Lin, J. Yang, H. Zhang and P. Chen, *Angew. Chem., Int. Ed.*, 2015, **54**, 4651–4656.
32 G. Z. Sun, L. X. Zheng, J. An, Y. Z. Pan, J. Y. Zhou, Z. Y. Zhan, J. H. L. Pang, C. K. Chua, K. F. Leong and L. Li, *Nanoscale*, 2013, **5**, 2870–2874.
33 Q. Qian, Q. Hu, L. Li, P. Shi, J. Zhou, J. Kong, X. Zhang, G. Sun and W. Huang, *Sens. Actuators, B*, 2018, **257**, 23–28.
34 J. D. Shi, X. M. Li, H. Y. Cheng, Z. J. Liu, L. Y. Zhao, T. T. Yang, Z. H. Dai, Z. G. Cheng, E. Z. Shi, L. Yang, Z. Zhang, A. Y. Cao, H. W. Zhu and Y. Fang, *Adv. Funct. Mater.*, 2016, **26**, 2078–2084.
35 Y. Wang, L. Wang, T. T. Yang, X. Li, X. B. Zang, M. Zhu, K. L. Wang, D. H. Wu and H. W. Zhu, *Adv. Funct. Mater.*, 2014, **24**, 4666–4670.
36 D. Kang, P. V. Pikhitsa, Y. W. Choi, C. Lee, S. S. Shin, L. F. Piao, B. Park, K. Y. Suh, T. I. Kim and M. Choi, *Nature*, 2014, **516**, 222–226.
37 J. Foroughi, G. M. Spinks, G. G. Wallace, J. Oh, M. E. Kozlov, S. L. Fang, T. Mirfakhrai, J. D. W. Madden, M. K. Shin, S. J. Kim and R. H. Baughman, *Science*, 2011, **334**, 494–497.
38 M. Behl, M. Y. Razzaq and A. Lendlein, *Adv. Mater.*, 2010, **22**, 3388–3410.
39 J. E. Deng, Y. Zhang, Y. Zhao, P. N. Chen, X. L. Cheng and H. S. Peng, *Angew. Chem., Int. Ed.*, 2015, **54**, 15419–15423.